

Prompt photon hadroproduction at high energies in off-shell gluon-gluon fusion

S.P. Baranov^a, A.V. Lipatov^b, N.P. Zotov^b

October 30, 2018

^a *P.N. Lebedev Physics Institute,
119991 Moscow, Russia*

^b *D.V. Skobeltsyn Institute of Nuclear Physics,
M.V. Lomonosov Moscow State University,
119991 Moscow, Russia*

Abstract

The amplitude for production of a single photon associated with quark pair in the fusion of two off-shell gluons is calculated. The matrix element found is applied to the inclusive prompt photon hadroproduction at high energies in the framework of k_T -factorization QCD approach. The total and differential cross sections are calculated in both central and forward pseudo-rapidity regions. The conservative error analysis is performed. We used the unintegrated gluon distributions in a proton which were obtained from the full CCFM evolution equation as well as from the Kimber-Martin-Ryskin prescription. Theoretical results were compared with recent experimental data taken by the DØ and CDF collaborations at Fermilab Tevatron. Theoretical predictions for the LHC energies are given.

PACS number(s): 12.38.-t, 13.85.-t

1 Introduction

The production of prompt (or direct) photons in hadron-hadron collisions at the Tevatron is a subject of intense studies [1–6]. Usually the photons are called "prompt" if they are coupled to the interacting quarks. The theoretical and experimental investigations of such processes have provided a direct probe of the hard subprocess dynamics, since the produced photons are largely insensitive to the effects of final-state hadronization. At the leading order, prompt photons can be produced via quark-gluon Compton scattering or quark-antiquark

annihilation [7] and so, the cross sections of these processes are strongly sensitive to the parton (quark and gluon) content of a proton¹. Very recently experimental data [6] on the inclusive prompt photon hadroproduction at the Tevatron have been presented by the DØ collaboration. These data extend previous measurements to significantly higher values of the photon p_T (namely to $p_T \sim 300$ GeV at $\sqrt{s} = 1960$ GeV). In the present paper we will analyse the data [1–6] using the so-called k_T -factorization [9, 10] (or semihard [11, 12]) approach of QCD.

The k_T -factorization approach is based on the familiar Balitsky-Fadin-Kuraev-Lipatov (BFKL) [13] or Ciafaloni-Catani-Fiorani-Marchesini (CCFM) [14] gluon evolution equations. In this way, the large logarithmic terms proportional to $\ln 1/x$ are summed up to all orders of perturbation theory (in the leading logarithm approximation). It is in contrast with the popular Dokshitzer-Gribov-Lipatov-Altarelli-Parizi (DGLAP) [15] strategy where only large logarithmic terms proportional to $\ln \mu^2$ are taken into account. The basic dynamical quantity of the k_T -factorization approach is the so-called unintegrated (i.e. \mathbf{k}_T -dependent) gluon distribution $\mathcal{A}(x, \mathbf{k}_T^2, \mu^2)$ which determines the probability to find a gluon carrying the longitudinal momentum fraction x and the transverse momentum \mathbf{k}_T at the probing scale μ^2 . The unintegrated gluon distribution can be obtained from the analytical or numerical solution of BFKL or CCFM equations. Similar to DGLAP, to calculate the cross sections of any physical process the unintegrated gluon density $\mathcal{A}(x, \mathbf{k}_T^2, \mu^2)$ has to be convoluted [9–12] with the relevant partonic cross section which has to be taken off mass shell (\mathbf{k}_T -dependent). It is in clear contrast with the usual DGLAP scheme (so-called collinear factorization). Since gluons in the initial state are not on-shell and are characterized by virtual masses (proportional to their transverse momentum), it also assumes a modification of their polarization density matrix [11, 12]. In particular, the polarization vector of a gluon is no longer purely transversal, but acquires an admixture of longitudinal and time-like components. Other important properties of the k_T -factorization formalism are the additional contribution to the cross sections due to the integration over the \mathbf{k}_T^2 region above μ^2 and the broadening of the transverse momentum distributions due to extra transverse momentum of the colliding partons.

It is important that at present a complete theoretical description of the prompt photon production data at the Tevatron is a subject of special investigations (see, for example, [16] and references therein). Both the completeness of next-to-leading order (NLO) perturbative QCD calculations [17] and consistency of the available data have been the subject of intense discussions [18–25]. Despite that the NLO pQCD predictions agree with the recent high- p_T measurements [6] within uncertainties, there are still open questions. So, it was found [1–4] that the shape of the measured cross sections as a function of photon transverse energy E_T is poorly described by the NLO pQCD calculations: the observed E_T distribution is steeper than the predictions of perturbative QCD. These shape differences lead to a significant disagreement in the ratio of cross sections calculated at different center-of-mass energies $\sqrt{s} = 630$ GeV and $\sqrt{s} = 1800$ GeV as a function of scaling variable $x_T = 2E_T^\gamma/\sqrt{s}$. It was claimed [2, 3] that the disagreement in the x_T ratio is difficult to explain with conventional theoretical uncertainties connected with the scale dependence and parametrizations of the parton distributions. The origin of the disagreement has been attributed to the effect of

¹Also observed photon may arise from so called fragmentation processes [8], where a final state quark or gluon decays into γ . This contribution will be discussed below in Section 2.

initial-state soft-gluon radiation [21, 22]. In the papers [22, 26] it was shown that the observed discrepancy can be reduced by introducing some additional intrinsic transverse momentum k_T of the incoming partons, which is usually assumed to have a Gaussian-like distribution. The average value of this k_T increases from $\langle k_T \rangle \sim 1$ GeV to more than $\langle k_T \rangle \sim 3$ GeV in hard-scattering processes as the \sqrt{s} increases from UA6 to Tevatron energies [22, 25]. The importance of including the gluon emission through the resummation formalism was recognized and only recently this approach has been developed for inclusive prompt photon production [26–30].

In the framework of k_T -factorization formalism the treatment of k_T -enhancement in the inclusive prompt photon hadroproduction at Tevatron suggests a modification of the above simple k_T smearing picture. In this approach the transverse momentum of incoming partons is generated in the course of non-collinear parton evolution under control of relevant evolution equations. In paper [18] the Kimber-Martin-Ryskin (KMR) formalism [31] (in the double leading logarithmic approximation) was applied to study the role of the both non-perturbative and perturbative components of partonic k_T in describing of the observed E_T spectrum. Note that this formalism is based on the standard DGLAP evolution. In calculations [18] the usual on-shell matrix elements of quark-gluon fusion and quark-antiquark annihilation were evaluated with precise off-shell kinematics. In our previous paper [32] we have used the proper off-shell expressions for the matrix elements of these partonic subprocesses and also the KMR-constructed unintegrated parton densities² (which were evaluated independently from other authors). Our predictions for the inclusive prompt photon production agree well with available DØ [1, 2] and CDF [3–5] experimental data at Tevatron in both central and forward pseudo-rapidity regions. Perfect agreement was found also in the ratio of two cross sections calculated at $\sqrt{s} = 630$ GeV and $\sqrt{s} = 1800$ GeV. This ratio shows specific effect connected with off-shell gluons in the k_T -factorization approach.

We note, however, that an important component of all above calculations [18, 32] is the unintegrated quark distribution in a proton. At present these densities are available in the framework of KMR approach only. It is because there are some theoretical difficulties in obtaining the quark distributions immediately from CCFM or BFKL equations³ (see, for example, review [35] for more details). As a result the dependence of the calculated cross sections on the non-collinear evolution scheme has not been investigated yet. This dependence in general can be significant and it is a special subject of study in the k_T -factorization formalism. Therefore in the present paper we will try a different and more systematic way. Instead of using the unintegrated quark distributions and the corresponding quark-gluon fusion and quark-antiquark annihilation cross sections we will calculate off-shell matrix element of the $g^*g^* \rightarrow q\bar{q}\gamma$ subprocess and then will operate in terms of the unintegrated gluon densities only. In this way the different non-collinear evolution schemes can be applied. But we note that this matrix element covers only sea quark contribution from the quark-gluon fusion and quark-antiquark annihilation and therefore in this case contribution from the valence quarks is not taken into account. However, this contribution is significant only at large x and therefore can be safely accounted for in the collinear LO approximation as additional one.

So, in the present paper we will investigate the different prompt photon production rates

²A similar scenario has been used also in [33].

³Unintegrated quark density was considered recently in [34].

using the off-mass shell matrix elements of the $g^*g^* \rightarrow q\bar{q}\gamma$ subprocess and make a systematic comparison of our predictions to the available DØ and CDF data [1–6]. Our special goal is to study the sensitivity of the calculated cross sections to the non-collinear evolution scheme. In the numerical calculations we will test the different sets of unintegrated gluon distributions which are obtained from the full CCFM equation as well as from the Kimber-Martin-Ryskin approach. Additionally we give some predictions for LHC conditions.

The outline of our paper is following. In Section 2 we recall shortly the basic formulas of the k_T -factorization approach with a brief review of calculation steps. In Section 3 we present the numerical results of our calculations and a discussion. Finally, in Section 4, we give some conclusions.

2 Theoretical framework

2.1 Kinematics

We start from the kinematics (see Fig. 1). Let $p^{(1)}$ and $p^{(2)}$ be the four-momenta of the incoming protons and p be the four-momentum of the produced photon. The initial off-shell gluons have the four-momenta k_1 and k_2 and the final quark and antiquark have the four-momenta p_1 and p_2 and masses m_q , respectively. In the $p\bar{p}$ center-of-mass frame we can write

$$p^{(1)} = \sqrt{s}/2 (1, 0, 0, 1), \quad p^{(2)} = \sqrt{s}/2 (1, 0, 0, -1), \quad (1)$$

where \sqrt{s} is the total energy of the process under consideration and we neglect the masses of the incoming protons. The initial gluon four-momenta in high energy limit can be written as

$$k_1 = x_1 p^{(1)} + k_{1T}, \quad k_2 = x_2 p^{(2)} + k_{2T}, \quad (2)$$

where k_{1T} and k_{2T} are their transverse four-momenta. It is important that $\mathbf{k}_{1T}^2 = -k_{1T}^2 \neq 0$ and $\mathbf{k}_{2T}^2 = -k_{2T}^2 \neq 0$. From the conservation laws we can easily obtain the following conditions:

$$\begin{aligned} \mathbf{k}_{1T} + \mathbf{k}_{2T} &= \mathbf{p}_{1T} + \mathbf{p}_{2T} + \mathbf{p}_T, \\ x_1 \sqrt{s} &= m_{1T} e^{y_1} + m_{2T} e^{y_2} + |\mathbf{p}_T| e^y, \\ x_2 \sqrt{s} &= m_{1T} e^{-y_1} + m_{2T} e^{-y_2} + |\mathbf{p}_T| e^{-y}, \end{aligned} \quad (3)$$

where y is the rapidity of produced photon, p_{1T} and p_{2T} are the transverse four-momenta of final quark and antiquark, y_1 , y_2 , m_{1T} and m_{2T} are their center-of-mass rapidities and transverse masses, i.e. $m_{iT}^2 = m_q^2 + \mathbf{p}_{iT}^2$.

2.2 Off-shell amplitude of the $g^*g^* \rightarrow q\bar{q}\gamma$ subprocess

There are eight Feynman diagrams (see Fig. 2) which describe the partonic subprocess $g^*g^* \rightarrow q\bar{q}\gamma$ at the leading order in α_s and α . Let ϵ_1 , ϵ_2 and ϵ be the initial gluon and produced photon polarization vectors, respectively, and a and b the eight-fold color indices of the off-shell gluons. Then the relevant matrix element can be presented as follows:

$$\mathcal{M}_1 = eg^2 \bar{u}(p_1) t^a \gamma^\mu \epsilon_\mu \frac{\hat{p}_1 - \hat{k}_1 + m_q}{m_q^2 - (p_1 - k_1)^2} \gamma^\lambda \epsilon_\lambda \frac{\hat{k}_2 - \hat{p}_2 + m_q}{m_q^2 - (k_2 - p_2)^2} t^b \gamma^\nu \epsilon_\nu u(p_2), \quad (4)$$

$$\mathcal{M}_2 = eg^2 \bar{u}(p_1) t^b \gamma^\nu \epsilon_\nu \frac{\hat{p}_1 - \hat{k}_2 + m_q}{m_q^2 - (p_1 - k_2)^2} \gamma^\lambda \epsilon_\lambda \frac{\hat{k}_1 - \hat{p}_2 + m_q}{m_q^2 - (k_1 - p_2)^2} t^a \gamma^\mu \epsilon_\mu u(p_2), \quad (5)$$

$$\mathcal{M}_3 = eg^2 \bar{u}(p_1) t^a \gamma^\mu \epsilon_\mu \frac{\hat{p}_1 - \hat{k}_1 + m_q}{m_q^2 - (p_1 - k_1)^2} t^b \gamma^\nu \epsilon_\nu \frac{-\hat{p}_2 - \hat{p} + m_q}{m_q^2 - (-p_2 - p)^2} \gamma^\lambda \epsilon_\lambda u(p_2), \quad (6)$$

$$\mathcal{M}_4 = eg^2 \bar{u}(p_1) t^b \gamma^\nu \epsilon_\nu \frac{\hat{p}_1 - \hat{k}_2 + m_q}{m_q^2 - (p_1 - k_2)^2} t^a \gamma^\mu \epsilon_\mu \frac{-\hat{p}_2 - \hat{p} + m_q}{m_q^2 - (-p_2 - p)^2} \gamma^\lambda \epsilon_\lambda u(p_2), \quad (7)$$

$$\mathcal{M}_5 = eg^2 \bar{u}(p_1) \gamma^\lambda \epsilon_\lambda \frac{\hat{p}_1 + \hat{p} + m_q}{m_q^2 - (p_1 + p)^2} t^b \gamma^\nu \epsilon_\nu \frac{\hat{k}_1 - \hat{p}_2 + m_q}{m_q^2 - (k_1 - p_2)^2} t^a \gamma^\mu \epsilon_\mu u(p_2), \quad (8)$$

$$\mathcal{M}_6 = eg^2 \bar{u}(p_1) \gamma^\lambda \epsilon_\lambda \frac{\hat{p}_1 + \hat{p} + m_q}{m_q^2 - (p_1 + p)^2} t^a \gamma^\mu \epsilon_\mu \frac{\hat{k}_2 - \hat{p}_2 + m_q}{m_q^2 - (k_2 - p_2)^2} t^b \gamma^\nu \epsilon_\nu u(p_2), \quad (9)$$

$$\begin{aligned} \mathcal{M}_7 = & eg^2 \bar{u}(p_1) \gamma^\rho C^{\mu\nu\rho}(k_1, k_2, -k_1 - k_2) \frac{\epsilon_\mu \epsilon_\nu}{(k_1 + k_2)^2} f^{abc} t^c \times \\ & \times \frac{-\hat{p}_2 - \hat{p} + m_q}{m_q^2 - (-p_2 - p)^2} \gamma^\lambda \epsilon_\lambda u(p_2), \end{aligned} \quad (10)$$

$$\begin{aligned} \mathcal{M}_8 = & eg^2 \bar{u}(p_1) \gamma^\lambda \epsilon_\lambda \frac{\hat{p}_1 + \hat{p} + m_q}{m_q^2 - (p_1 + p)^2} \times \\ & \times \gamma^\rho C^{\mu\nu\rho}(k_1, k_2, -k_1 - k_2) \frac{\epsilon_\mu \epsilon_\nu}{(k_1 + k_2)^2} f^{abc} t^c u(p_2). \end{aligned} \quad (11)$$

In above expressions $C^{\mu\nu\rho}(k, p, q)$ is related to the standard QCD three-gluon coupling

$$C^{\mu\nu\rho}(k, p, q) = g^{\mu\nu}(p - k)^\rho + g^{\nu\rho}(q - p)^\mu + g^{\rho\mu}(k - q)^\nu. \quad (12)$$

The summation on the produced photon polarization is carried out by covariant formula

$$\sum \epsilon^\mu \epsilon^{*\nu} = -g^{\mu\nu}. \quad (13)$$

In the case of initial off-shell gluon we use the BFKL prescription [11–13]:

$$\epsilon^\mu(k) \epsilon^{*\nu}(k) = \frac{k_T^\mu k_T^\nu}{\mathbf{k}_T^2}. \quad (14)$$

This formula converges to the usual one (13) after azimuthal angle averaging in the $k_T \rightarrow 0$ limit. The evaluation of the traces in (4) — (11) was done using the algebraic manipulation system FORM [36]. The usual method of squaring of (4) — (11) results in enormously long output. This technical problem was solved by applying the method of orthogonal amplitudes [37].

The gauge invariance of matrix element is a subject of special attention in the k_T -factorization approach. Strictly speaking, the diagrams shown in Fig. 2 are insufficient and have to be accompanied with the graphs involving direct gluon exchange between the protons (these protons are not shown in Fig. 2). These graphs are necessary to maintain the gauge invariance. However, they violate the factorization since they cannot be represented as a convolution of gluon-gluon fusion matrix element with unintegrated gluon density. The

solution pointed out in [10] refers to the fact that, within the particular gauge (13), the contribution from these unfactorizable diagrams vanish, and one has to only take into account the graphs depicted in Fig. 2. We have successfully tested the gauge invariance of matrix element (4) — (11) numerically.

2.3 Fragmentation contributions

Perturbation theory becomes nonapplicable when the wavelength of the emitted photon (in the emitting quark rest frame) becomes larger than the typical hadronic scale $\mathcal{O}(1 \text{ GeV}^{-1})$. Then the nonperturbative effects of hadronization or fragmentation must be taken into account. Accordingly, the calculated cross section can be split into two pieces

$$d\sigma = d\sigma_{\text{direct}}(\mu^2) + d\sigma_{\text{fragm}}(\mu^2)$$

with $d\sigma_{\text{direct}}(\mu^2)$ representing the perturbative contribution and $d\sigma_{\text{fragm}}(\mu^2)$ the fragmentation contribution. In our calculations we choose the fragmentation scale μ^2 to be the invariant mass of the quark + photon subsystem, $\mu^2 = (p + p_i)^2$, and restrict $d\sigma_{\text{direct}}(\mu^2)$ to $\mu \geq M \simeq 1 \text{ GeV}$. Under this condition, the contribution $d\sigma_{\text{direct}}(\mu^2)$ is free from divergences, so that the mass of the light quark m_q can be safely sent to zero. The sensitivity of our results to the choice of M is reasonably soft, as we will discuss in Section 3. As far as the fragmentation contribution is concerned, its size is dramatically reduced by the photon isolation cuts (see below). According to the estimates presented in Ref. [38], the contribution from $d\sigma_{\text{fragm}}$ amounts to about 10% of the visible cross section. This value is smaller than the theoretical uncertainty in calculating the perturbative contribution $d\sigma_{\text{direct}}$, and so, is neglected in our analysis.

2.4 Photon isolation cuts

In order to reduce huge background from the secondary photons produced by the decays of π^0 and η mesons the isolation criterion is introduced in the experimental analyses. This criterion is the following. A photon is isolated if the amount of hadronic transverse energy E_T^{had} , deposited inside a cone with aperture R centered around the photon direction in the pseudo-rapidity and azimuthal angle plane, is smaller than some value E_T^{max} :

$$\begin{aligned} E_T^{\text{had}} &\leq E_T^{\text{max}}, \\ (\eta^{\text{had}} - \eta)^2 + (\phi^{\text{had}} - \phi)^2 &\leq R^2. \end{aligned} \tag{15}$$

The both DØ and CDF collaborations take $R \sim 0.4$ and $E_T^{\text{max}} \sim 1 \text{ GeV}$ in the experiment [1–6]. Isolation not only reduces the background but also significantly reduces the fragmentation components connected with collinear photon radiation. It was shown that after applying the isolation cut (15) the contribution from the fragmentation subprocesses is strongly suppressed [38].

2.5 Cross section for prompt photon hadroproduction

In general case, according to k_T -factorization theorem the cross section of prompt photon hadroproduction can be written as a convolution

$$\begin{aligned} \sigma(p\bar{p} \rightarrow \gamma X) &= \sum_q \int \frac{dx_1}{x_1} \mathcal{A}(x_1, \mathbf{k}_{1T}^2, \mu^2) d\mathbf{k}_{1T}^2 \frac{d\phi_1}{2\pi} \times \\ &\times \int \frac{dx_2}{x_2} \mathcal{A}(x_2, \mathbf{k}_{2T}^2, \mu^2) d\mathbf{k}_{2T}^2 \frac{d\phi_2}{2\pi} d\hat{\sigma}(g^* g^* \rightarrow q\bar{q}\gamma), \end{aligned} \quad (16)$$

where $\hat{\sigma}(g^* g^* \rightarrow q\bar{q}\gamma)$ is the partonic cross section, $\mathcal{A}(x, \mathbf{k}_T^2, \mu^2)$ is the unintegrated gluon distribution in a proton and ϕ_1 and ϕ_2 are the azimuthal angles of the incoming gluons. The multiparticle phase space $\Pi d^3p_i / 2E_i \delta^{(4)}(\sum p^{\text{in}} - \sum p^{\text{out}})$ is parametrized in terms of transverse momenta, rapidities and azimuthal angles:

$$\frac{d^3p_i}{2E_i} = \frac{\pi}{2} d\mathbf{p}_{iT}^2 dy_i \frac{d\phi_i}{2\pi}. \quad (17)$$

Using the expressions (16) and (17) we can easily obtain the master formula:

$$\begin{aligned} \sigma(p\bar{p} \rightarrow \gamma X) &= \sum_q \int \frac{1}{256\pi^3 (x_1 x_2 s)^2} |\bar{\mathcal{M}}(g^* g^* \rightarrow q\bar{q}\gamma)|^2 \times \\ &\times \mathcal{A}(x_1, \mathbf{k}_{1T}^2, \mu^2) \mathcal{A}(x_2, \mathbf{k}_{2T}^2, \mu^2) d\mathbf{k}_{1T}^2 d\mathbf{k}_{2T}^2 d\mathbf{p}_{1T}^2 d\mathbf{p}_{2T}^2 dy dy_1 dy_2 \frac{d\phi_1}{2\pi} \frac{d\phi_2}{2\pi} \frac{d\psi_1}{2\pi} \frac{d\psi_2}{2\pi}, \end{aligned} \quad (18)$$

where $|\bar{\mathcal{M}}(g^* g^* \rightarrow q\bar{q}\gamma)|^2$ is the off-mass shell matrix element squared and averaged over initial gluon polarizations and colors, ψ_1 and ψ_2 are the azimuthal angles of the final state quark and antiquark, respectively. We would like to point out again that $|\bar{\mathcal{M}}(g^* g^* \rightarrow q\bar{q}\gamma)|^2$ is strongly depends on the non-zero transverse momenta \mathbf{k}_{1T}^2 and \mathbf{k}_{2T}^2 . If we average the expression (18) over ϕ_1 and ϕ_2 and take the limit $\mathbf{k}_{1T}^2 \rightarrow 0$ and $\mathbf{k}_{2T}^2 \rightarrow 0$, then we recover the expression for the prompt photon hadroproduction in the usual collinear approximation.

The multidimensional integration in (18) has been performed by the means of Monte Carlo technique, using the routine VEGAS [39]. The full C++ code is available from the authors on request⁴.

3 Numerical results

3.1 Theoretical uncertainties

Except the the unintegrated gluon distribution in a proton $\mathcal{A}(x, \mathbf{k}_T^2, \mu^2)$, there are several parameters which determined the overall normalization factor of the cross section (18): the quark mass m_q , the factorization and normalisation scales μ_F and μ_R .

Concerning the unintegrated gluon densities in a proton, we have tried here two different sets of them. These sets are widely discussed in the literature (see, for example, review [35] for more information). Here we only shortly discuss their characteristic properties.

⁴lipatov@theory.sinp.msu.ru

First unintegrated gluon density used has been obtained [40] recently from the numerical solution of the full CCFM equation. Function $\mathcal{A}(x, \mathbf{k}_T^2, \mu^2)$ is determined by a convolution of the non-perturbative starting distribution $\mathcal{A}_0(x)$ and the CCFM evolution denoted by $\tilde{\mathcal{A}}(x, \mathbf{k}_T^2, \mu^2)$:

$$\mathcal{A}(x, \mathbf{k}_T^2, \mu^2) = \int \frac{dx'}{x'} \mathcal{A}_0(x') \tilde{\mathcal{A}}\left(\frac{x}{x'}, \mathbf{k}_T^2, \mu^2\right). \quad (19)$$

In the perturbative evolution the gluon splitting function $P_{gg}(z)$ including non-singular terms (as described in detail in [41]) is applied. The input parameters in $\mathcal{A}_0(x)$ were fitted to describe the proton structure function $F_2(x, Q^2)$. A acceptable fit to the measured F_2 values was obtained with $\chi^2/ndf = 1.83$ using statistical and uncorrelated systematical uncertainties (compare to $\chi^2/ndf \sim 1.5$ in the collinear approach at NLO). This distribution has been applied recently in the analysis of the deep inelastic proton structure functions F_2^c , F_2^b and F_L [42].

Another set (the so-called KMR distribution) is the one which was originally proposed in [31]. The KMR approach is the formalism to construct unintegrated gluon distribution from the known conventional parton (quark and gluon) densities. It accounts for the angular-ordering (which comes from the coherence effects in gluon emission) as well as the main part of the collinear higher-order QCD corrections. The key observation here is that the μ dependence of the unintegrated parton distribution enters at the last step of the evolution. In the numerical calculations we have used the standard GRV (LO) parametrizations [43] of the collinear quark and gluon densities. The KMR-constructed parton distributions were used, in particular, to describe the prompt photon photoproduction at HERA [44] and prompt photon hadroproduction Tevatron [32].

Significant theoretical uncertainties are connected with the choice of the factorization and renormalization scales. The first of them is related to the evolution of the gluon distributions, the other is responsible for the strong coupling constant $\alpha_s(\mu_R^2)$. As it often done, we choose the renormalization and factorization scales to be equal: $\mu_R = \mu_F = \mu = \xi |\mathbf{p}_T|$. In order to investigate the scale dependence of our results we will vary the scale parameter ξ between 1/2 and 2 about the default value $\xi = 1$.

The masses of all light quarks were set to be equal to $m_q = 4.5$ MeV and the charmed quark mass was set to $m_c = 1.4$ GeV. We have checked that uncertainties which come from these quantities are negligible in comparison to the uncertainties connected with the unintegrated gluon distributions. For completeness, we use LO formula for the strong coupling constant $\alpha_s(\mu^2)$ with $n_f = 3$ active quark flavours at $\Lambda_{\text{QCD}} = 232$ MeV, such that $\alpha_s(M_Z^2) = 0.117$. Note that we use special choice $n_f = 4$ and $\Lambda_{\text{QCD}} = 130$ MeV in the case of CCFM gluon ($\alpha_s(M_Z^2) = 0.118$), as it was originally proposed in [40].

3.2 Inclusive prompt photon production at Tevatron

The experimental data [1–6] for the inclusive prompt photon hadroproduction $p\bar{p} \rightarrow \gamma X$ at Tevatron come from both the DØ and CDF collaborations. The DØ [1, 2] data were obtained in the central and forward pseudo-rapidity regions for two different center-of-mass energies, namely $\sqrt{s} = 630$ GeV and $\sqrt{s} = 1800$ GeV. The central pseudo-rapidity region is defined by the requirement $|\eta| < 0.9$, and the forward one is defined by $1.6 < |\eta| < 2.5$. The more recent CDF data [3, 4] refer to the same central kinematical region $|\eta| < 0.9$ for both

beam energies $\sqrt{s} = 630$ GeV and $\sqrt{s} = 1800$ GeV. As usually, the photon pseudo-rapidity η is defined as $\eta = -\ln \tan(\theta/2)$, where θ is the polar angle of the prompt photon with respect to the proton beam. Also the CDF collaboration has presented a measurement [5] of the prompt photon cross section at $\sqrt{s} = 1800$ GeV which is based on events where the photon converts into an electron-positron pair in the material of inner detector, resulting in a two track event signature ("conversion" data). These data refer only to the central kinematical region. Actually, there are two different datasets, which were used in the CDF measurement with conversions, namely 8 GeV electron data and 23 GeV photon data⁵. Last available experimental data has been presented by the DØ collaboration very recently [6]. These data extend previous measurements [1–5] to significantly higher values of photon p_T (namely to $p_T \sim 300$ GeV at $\sqrt{s} = 1960$ GeV).

The results of our calculations are shown in Figs. 3 — 18. So, Figs. 3 and 4 confront the double differential cross sections $d\sigma/dE_T d\eta$ calculated at $\sqrt{s} = 630$ GeV in different kinematical regions with the DØ [2] and CDF [3] data. The solid and dotted lines are obtained by using the CCFM and KMR unintegrated gluon densities with the default factorization and renormalization scale. The upper and lower dashed lines correspond to the scale variations in CCFM gluon as it was described above. The data/theory ratio is also shown in Figs. 5 and 6. One can see that our predictions agree well with the experimental data within the scale uncertainties. However, the results of calculation with the KMR gluon at the default scale tend to underestimate the data in the central kinematical region and agree with the DØ data in the forward η region. The CCFM gluon density gives a perfect description of the data in both kinematical regions. Main difference in predictions of the KMR and CCFM gluon densities concentrated in the central pseudo-rapidity region at low p_T . This region corresponds to the low x values where effects of the gluon evolution play the dominant role. It is clear from the Figs. 7 and 8 where gluon and valence quark contributions are shown separately. In the central pseudo-rapidity region the gluon-gluon fusion dominates up to $p_T \sim 20$ GeV approximately whereas in the forward pseudo-rapidity region the valence quark contribution should be taken into account everywhere. In these plots we have used the CCFM gluon density for illustration. Note that the KMR gluon give description of the data which is rather similar to collinear NLO QCD calculations [17]: the results of measurement are higher than the NLO prediction at low E_T in the central η range but agree at all E_T in the forward pseudo-rapidity region.

It is important that KMR predictions based on the $g^*g^* \rightarrow q\bar{q}\gamma$ off-shell matrix element practically coincide with the previous ones [32] which were based on the quark-gluon fusion and quark-antiquark annihilation. This fact gives an additional check of our calculations and the self-consistency of the whole KMR scheme.

The double differential cross sections $d\sigma/dE_T d\eta$ compared with the experimental data at $\sqrt{s} = 1800$ GeV in different pseudo-rapidity regions are shown in Figs. 9 — 11. The data/theory ratio is depicted in Figs. 12 and 13. The gluon and valence quark contributions to the cross section at this energy are shown separately in Fig. 14 and 15. We find that our predictions with CCFM gluon density reasonable agree with the DØ [1] and CDF [3–5] data both in normalization and shape. However, the using of the KMR-evolved gluon density results to underestimation of the measurement by a factor about 2 in the central η region.

⁵See Ref. [5] for more details.

The similar situation is observed at $\sqrt{s} = 1960$ GeV (see Fig. 16). This is due to different small- x behaviour of the unintegrated gluon densities, since valence quark contribution in this region is about 7% only, as it was demonstrated in Fig. 14. In forward pseudo-rapidity region the results obtained with the both gluon densities under consideration agree well with the experimental data. So one can conclude that in the central pseudo-rapidity region at low p_T the observed cross section is a strongly sensitive to the unintegrated gluon density used. Therefore available experimental data can be applied in future to better constraint of the unintegrated gluon distribution. Specially it will be useful in the case of the CCFM evolution (which is valid for both small and large values of x) since measurements [1–6] on the prompt photon production refers to whole x range. One can see that the gluon-gluon contribution at $\sqrt{s} = 1800$ GeV dominates up to $p_T \sim 50$ GeV in the central η region and up to $p_T \sim 20$ GeV in the forward one, where x is small still. In general, the contribution from valence quarks is more significant in the forward rapidity region. This situation is the similar to one at $\sqrt{s} = 630$ GeV.

Concerning the collinear approximation of QCD, it was shown [6] that results from NLO calculations agree with the recent high p_T measurement within uncertainties. However, at moderate and small p_T region (which corresponds to small values of x) the shape of the measured cross sections at $\sqrt{s} = 1800$ GeV is generally steeper than that of the NLO predictions. It was claimed [3, 4] that this shape difference is difficult to explain simply by changing the renormalization/factorization scales in the collinear calculation, or the set of parton distribution functions.

Now we can try to extrapolate our theoretical predictions to LHC energies. We perform the calculation for both central and forward photon pseudo-rapidities η . As a representative example, we will define the central and forward kinematical regions by the requirements $|\eta| < 2.5$ and $2.5 < |\eta| < 4$, respectively. The transverse energy E_T distributions of inclusive prompt photon production at $\sqrt{s} = 14$ TeV are shown in Figs. 17 and 18. The formulas (15) were used in these predictions. These Figs show the size of theoretical uncertainties connected with the unintegrated gluon densities. It is worth mentioning that the extrapolation of the available parton distribution to the region of lower x is a special problem at the LHC energies. In particular, one of the problem is connected with the correct treatment of saturation effects in small x region⁶. Therefore additional work needs to be done until these uncertainties will be reduced.

4 Conclusions

We have tried a new theoretical approach to the production of prompt photons in hadronic collisions at high energies. Our approach is based on the k_t -factorization scheme, which, unlike many early calculations [21, 22, 25], provides solid theoretical grounds for adequately taking into account the effects of initial parton momentum. The central part of our consideration is the off-shell gluon-gluon fusion subprocess $g^*g^* \rightarrow q\bar{q}\gamma$. The corresponding off-shell matrix elements have been calculated for the first time. At the price of considering the $2 \rightarrow 3$ rather than $2 \rightarrow 2$ matrix elements, we have reduced the problem of unknown unintegrated quark distributions to the problem of gluon distributions. This way enables us with making

⁶See, for example, Ref. [35]

comparisons between the different parton evolution schemes and parametrizations of parton densities, in contrast with previous calculations [18, 32] where such a comparison was not possible (for the lack of unintegrated quark distributions except KMR).

Since the gluons are only responsible for the appearance of sea, but not valence quarks, the contribution from the valence quarks has been calculated separately. Having in mind that the valence quarks are only important at large x , where the traditional DGLAP evolution is accurate and reliable, we have calculated this contribution within the usual collinear scheme based on $2 \rightarrow 2$ partonic subprocesses and on-shell parton densities.

We have calculated the total and differential cross sections and have made comparisons to the recent DØ and CDF experimental data. In the numerical analysis we have used the unintegrated gluon densities which are obtained from the full CCFM equation as well as from the KMR prescription. We have found that in the central pseudo-rapidity region at low p_T the observed cross section is strongly sensitive to the unintegrated gluon density. In this kinematic region the cross sections evaluated with CCFM and KMR gluon distributions differ from each other by a factor of about 2. This is due to the fact that low- p_T measurements in the central pseudo-rapidity region probe the small- x region, where the shapes of the considered gluon densities are different. In the forward pseudo-rapidity region the predictions from different gluon densities practically coincide. We have demonstrated that the available experimental data can be used to constrain the unintegrated gluon distributions. Especially, it may be useful in the case of CCFM evolution (which is valid for both small and large values of x) since the recent DØ and CDF measurements cover the whole x range.

Our results based on Kimber-Martin-Ryskin [31] gluon density and off-shell gluon-gluon fusion matrix element $g^*g^* \rightarrow q\bar{q}\gamma$ agree with the previous results [32] based on the quark-gluon fusion $qg \rightarrow q\gamma$ and quark-antiquark annihilation $q\bar{q} \rightarrow g\gamma$ matrix elements and KMR [31] off-shell quark and gluon distributions. This can be regarded as an additional proof of the consistency of the proposed method.

5 Acknowledgements

We thank H. Jung for encouraging interest, very helpful discussions and for providing the CCFM code for unintegrated gluon distributions. The authors are very grateful to P.F. Ermolov for the support and DESY Directorate for the support in the framework of Moscow — DESY project on Monte-Carlo implementation for HERA — LHC. A.V.L. was supported in part by the grants of the president of Russian Federation (MK-9820.2006.2) and Helmholtz — Russia Joint Research Group. Also this research was supported by the FASI of Russian Federation (grant NS-8122.2006.2).

References

- [1] B. Abbott *et al.* (DØ Collaboration), Phys. Rev. Lett. **84**, 2786 (2000).
- [2] V.M. Abazov *et al.* (DØ Collaboration), Phys. Rev. Lett. **87**, 251805 (2001).
- [3] D. Acosta *et al.* (CDF Collaboration), Phys. Rev. **D65**, 112003 (2002).

- [4] D. Acosta *et al.* (CDF Collaboration), Phys. Rev. **D70**, 032001 (2004).
- [5] T. Affolder *et al.* (CDF Collaboration), Phys. Rev. **D65**, 012003 (2002).
- [6] V.M. Abazov *et al.* (DØ Collaboration), Phys. Lett. **639**, 151 (2006).
- [7] W. Vogelsang and A. Vogt, Nucl. Phys. **B453**, 334 (1995).
- [8] K. Koller, T.F. Walsh, and P.M. Zerwas, Z. Phys. **C2**, 197 (1979).
- [9] S. Catani, M. Ciafaloni, and F. Hautmann, Nucl. Phys. **B366**, 135 (1991).
- [10] J.C. Collins and R.K. Ellis, Nucl. Phys. **B360**, 3 (1991).
- [11] V.N. Gribov, E.M. Levin, and M.G. Ryskin, Phys. Rep. **100**, 1 (1983).
- [12] E.M. Levin, M.G. Ryskin, Yu.M. Shabelsky, and A.G. Shuvaev, Sov. J. Nucl. Phys. **53**, 657 (1991).
- [13] E.A. Kuraev, L.N. Lipatov, and V.S. Fadin, Sov. Phys. JETP **44**, 443 (1976);
E.A. Kuraev, L.N. Lipatov, and V.S. Fadin, Sov. Phys. JETP **45**, 199 (1977);
I.I. Balitsky and L.N. Lipatov, Sov. J. Nucl. Phys. **28**, 822 (1978).
- [14] M. Ciafaloni, Nucl. Phys. **B296**, 49 (1988);
S. Catani, F. Fiorani, and G. Marchesini, Phys. Lett. **B234**, 339 (1990);
S. Catani, F. Fiorani, and G. Marchesini, Nucl. Phys. **B336**, 18 (1990);
G. Marchesini, Nucl. Phys. **B445**, 49 (1995).
- [15] V.N. Gribov and L.N. Lipatov, Yad. Fiz. **15**, 781 (1972);
L.N. Lipatov, Sov. J. Nucl. Phys. **20**, 94 (1975);
G. Altarelli and G. Parizi, Nucl. Phys. **B126**, 298 (1977);
Y.L. Dokshitzer, Sov. Phys. JETP **46**, 641 (1977).
- [16] U. Baur *et al.*, "Report of the Working Group on Photon and Weak Boson Production, Batavia 1999, QCD and Weak Boson Physics in Run II" [hep-ph/0005226].
- [17] H.-N. Li, Phys. Lett. **B454**, 328 (1999);
T. Binoth, J.Ph. Guillet, E. Pilon, and M. Werlen, Eur. Phys. J. **C16**, 311 (2000);
S. Catani, M. Fontannaz, J.Ph. Guillet, and E. Pilon, JHEP **05**, 028 (2002);
L.E. Gordon and W. Vogelsang, Phys. Rev. **D48**, 3136 (1993).
- [18] M.A. Kimber, A.D. Martin, and M.G. Ryskin, Eur. Phys. J. **C12**, 655 (2000).
- [19] A.D. Martin, R.G. Roberts, W.J. Stirling, and R.S. Thorne, Eur. Phys. J. **C4**, 463 (1998).
- [20] H. Baer and M.H. Reno, Phys. Rev. **D54**, 2017 (1996).
- [21] J. Huston *et al.* (CTEQ Collaboration), Phys. Rev. **D51**, 6139 (1995).

- [22] L. Apanasevich, C. Balazs, C. Bromberg, J. Huston, A. Maul, W.K. Tung, S. Kuhlmann, J. Owens, M. Begel, T. Ferbel, G. Ginther, P. Slattery, and M. Zielinski, Phys. Rev. **D59**, 074007 (1999).
- [23] P. Aurenche, M. Fontannaz, J.Ph. Guillet, B.A. Kniehl, E. Pilon, and M. Werlen, Eur. Phys. J. **C9**, 107 (1999).
- [24] P. Aurenche, M. Fontannaz, J.Ph. Guillet, B.A. Kniehl, and M. Werlen, Eur. Phys. J. **C13**, 347 (2000).
- [25] A. Kumar, K. Ranjan, M.K. Jha, A. Bhardwaj, B.M. Sodermark, and R.K. Shivpuri, Phys. Rev. **D68**, 014017 (2003).
- [26] H.-L. Lai and H.-N. Li, Phys. Rev. **D58**, 114020 (1998).
- [27] S. Catani, M.L. Mangano, P. Nason, C. Oleari, and W. Vogelsang, JHEP **9903**, 025 (1999).
- [28] N. Kidonakis and J.F. Owens, Phys. Rev. **D61**, 094004 (2000).
- [29] E. Laenen, G. Oderda, and G. Sterman. Phys. Lett. **B438**, 173 (1998).
- [30] E. Laenen, G. Sterman, and W. Vogelsang, Phys. Rev. Lett. **84**, 4296 (2000).
- [31] M.A. Kimber, A.D. Martin, and M.G. Ryskin, Phys. Rev. **D63**, 114027 (2001);
G. Watt, A.D. Martin, and M.G. Ryskin, Eur. Phys. J. **C31**, 73 (2003).
- [32] A.V. Lipatov and N.P. Zotov, J. Phys. **G34**, 219 (2007);
S. Chekanov *et al.* (ZEUS Collaboration), Eur. Phys. J. **C49**, 511 (2007).
- [33] T. Pietrycki and A. Szczurek, Phys. Rev. **D75**, 014023 (2007);
T. Pietrycki and A. Szczurek, Phys. Rev. **D76**, 034003 (2007).
- [34] A.V. Bogdan and A.V. Grabovsky, Nucl. Phys. **B773**, 65 (2007).
- [35] B. Andersson *et al.* (Small- x Collaboration), Eur. Phys. J. **C25**, 77 (2002);
J. Andersen *et al.* (Small- x Collaboration), Eur. Phys. J. **C35**, 67 (2004);
J. Andersen *et al.* (Small- x Collaboration), Eur. Phys. J. **C48**, 53 (2006).
- [36] J.A.M. Vermaseren, "Symbolic Manipulation with FORM", published by Computer Algebra Nederland, Kruislaan 413, 1098, SJ Amsterdam, 1991; ISBN 90-74116-01-9.
- [37] R.E. Prange, Phys. Rev. **110**, 240 (1958);
S.P. Baranov, Phys. Atom. Nucl. **60**, 1322 (1997).
- [38] H. Baer, J. Ohnemus, and J.F. Owens, Phys. Rev. **D42**, 61 (1990);
P. Aurenche, M. Fontannaz, J.Ph. Guillet, E. Pilot, and M. Werlen, Phys. Rev. **D73**, 094007 (2006).
- [39] G.P. Lepage, J. Comput. Phys. **27**, 192 (1978).

- [40] H. Jung, A.V. Kotikov, A.V. Lipatov, and N.P. Zotov, in Proceedings of ICHEP'2006, p. 493 [hep-ph/0611093].
- [41] H. Jung, Mod. Phys. Lett. A **19**, 1 (2004).
- [42] H. Jung, A.V. Kotikov, A.V. Lipatov, and N.P. Zotov, in Proceedings of DIS'2007, p. 349 arXiv:0706.3793 [hep-ph].
- [43] M. Glück, E. Reya, and A. Vogt, Phys. Rev. **D46**, 1973 (1992);
M. Glück, E. Reya, and A. Vogt, Z. Phys. **C67**, 433 (1995).
- [44] A.V. Lipatov and N.P. Zotov, Phys. Rev. **D72**, 054002 (2005).
- [45] H. Jung, Comput. Phys. Comm. **143**, 100 (2002).

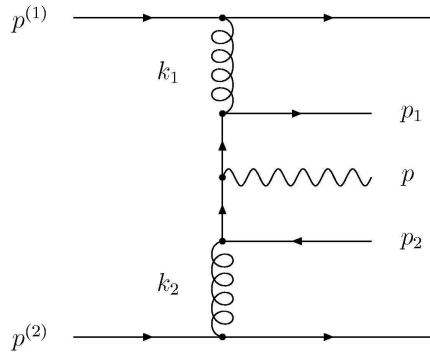


Figure 1: Kinematics of the $g^* g^* \rightarrow q \bar{q} \gamma$ process.

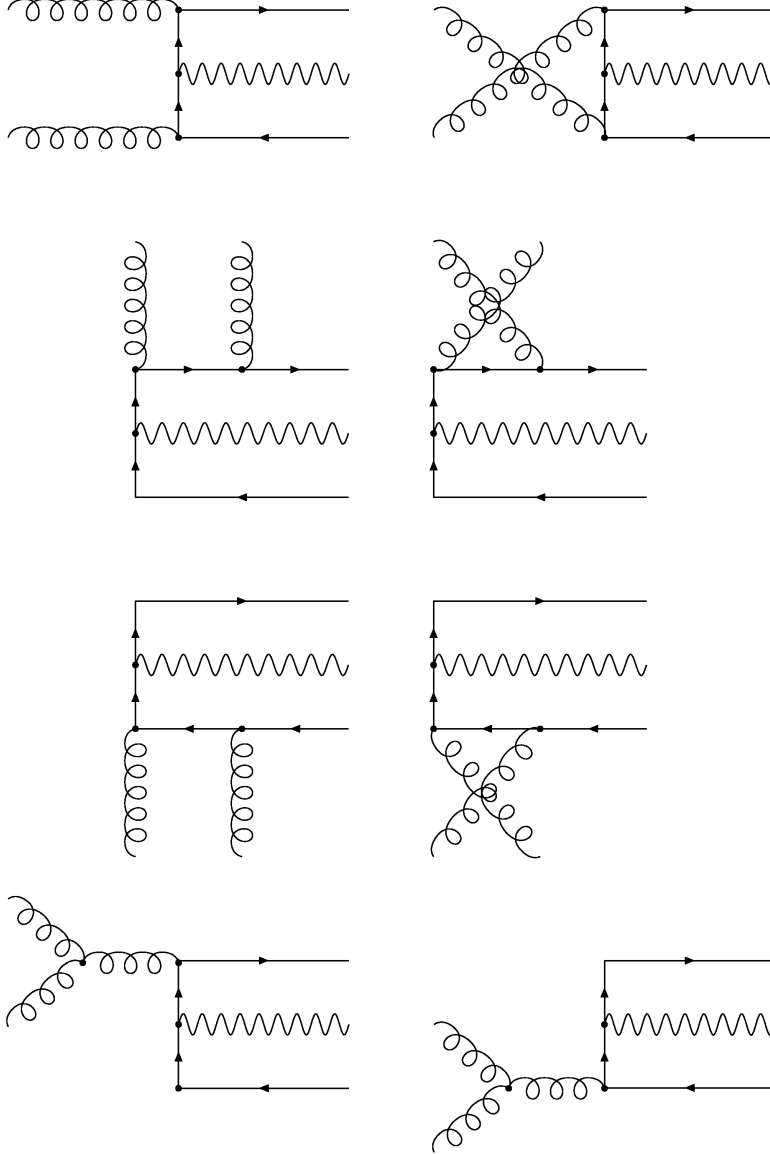


Figure 2: Feynman diagrams which describe the partonic subprocess $g^*g^* \rightarrow q\bar{q}\gamma$ at the leading order in α_s and α .

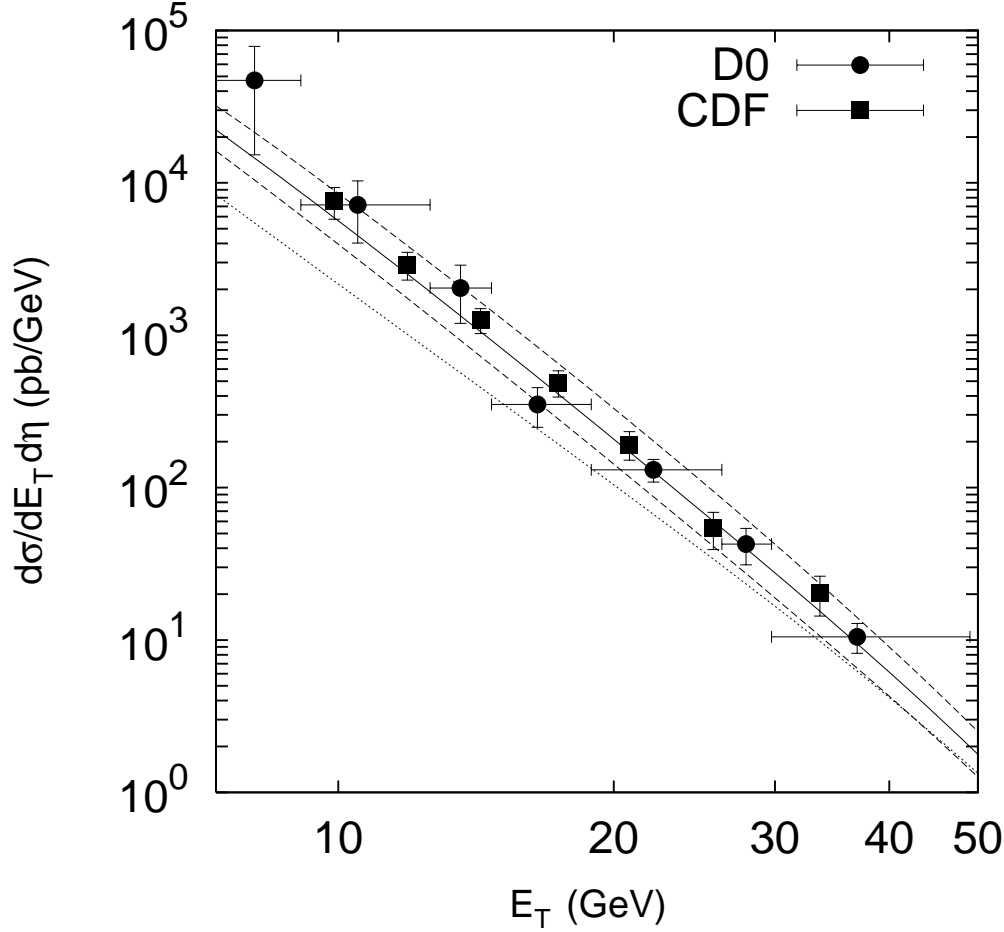


Figure 3: The double differential cross section $d\sigma/dE_T d\eta$ for inclusive prompt photon hadroproduction at $|\eta| < 0.9$ and $\sqrt{s} = 630$ GeV. The solid line corresponds to the CCFM gluon density with the default scale $\mu = E_T$, whereas upper and lower dashed lines correspond to the usual scale variation in the CCFM distribution, respectively. The dotted line corresponds to the KMR unintegrated gluon density. The experimental data are from DØ [2] and CDF [3].

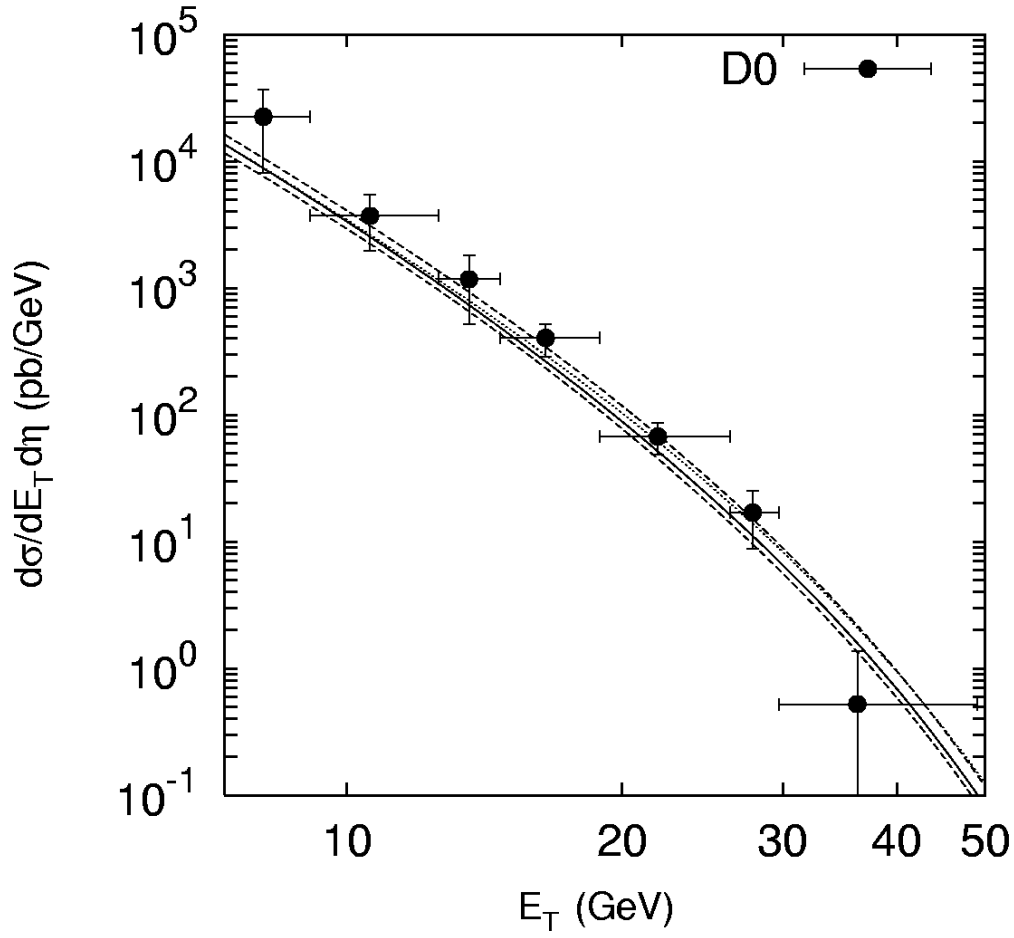


Figure 4: The double differential cross section $d\sigma/dE_T d\eta$ for inclusive prompt photon hadroproduction at $1.6 < |\eta| < 2.5$ and $\sqrt{s} = 630$ GeV. Notations of all curves are the same as in Figure 3. The experimental data are from D0 [2].

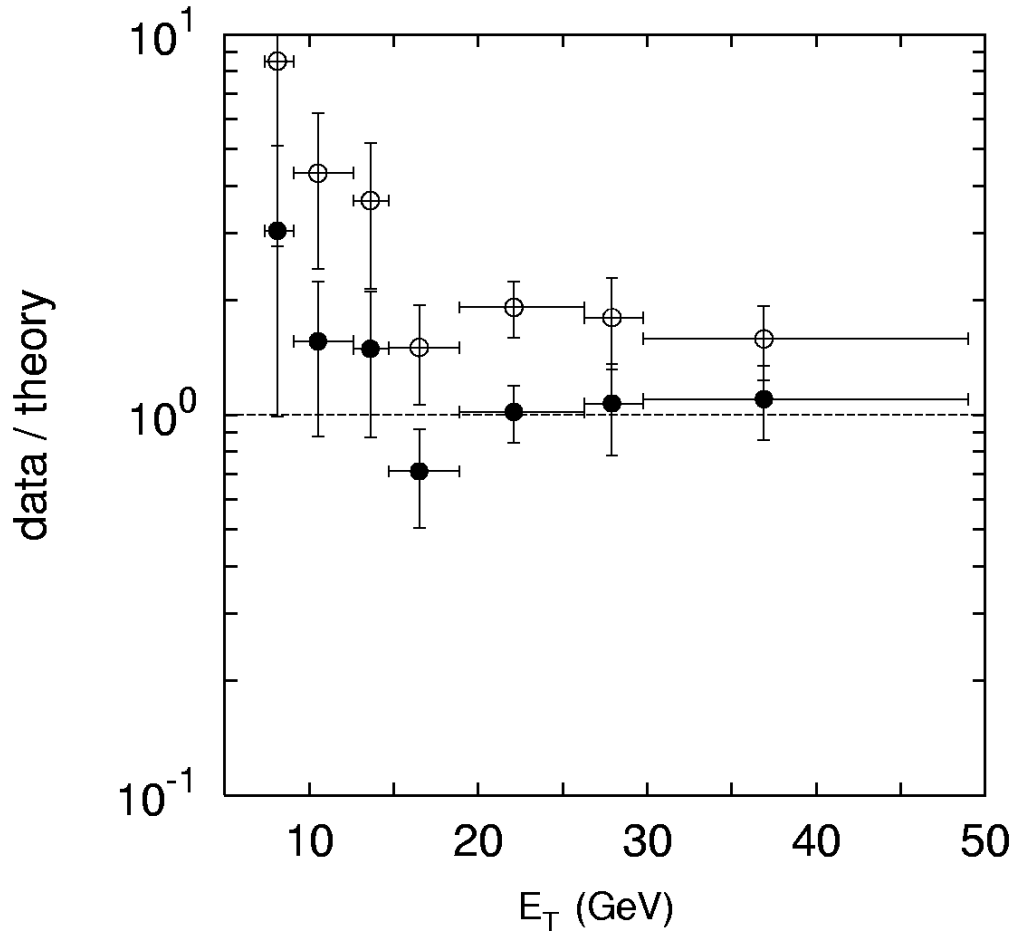


Figure 5: The data/theory ratio for inclusive prompt photon hadroproduction calculated at $|\eta| < 0.9$ and $\sqrt{s} = 630$ GeV. Black and open circles correspond to the CCFM and KMR gluon densities, respectively. The experimental data are from DØ [2].

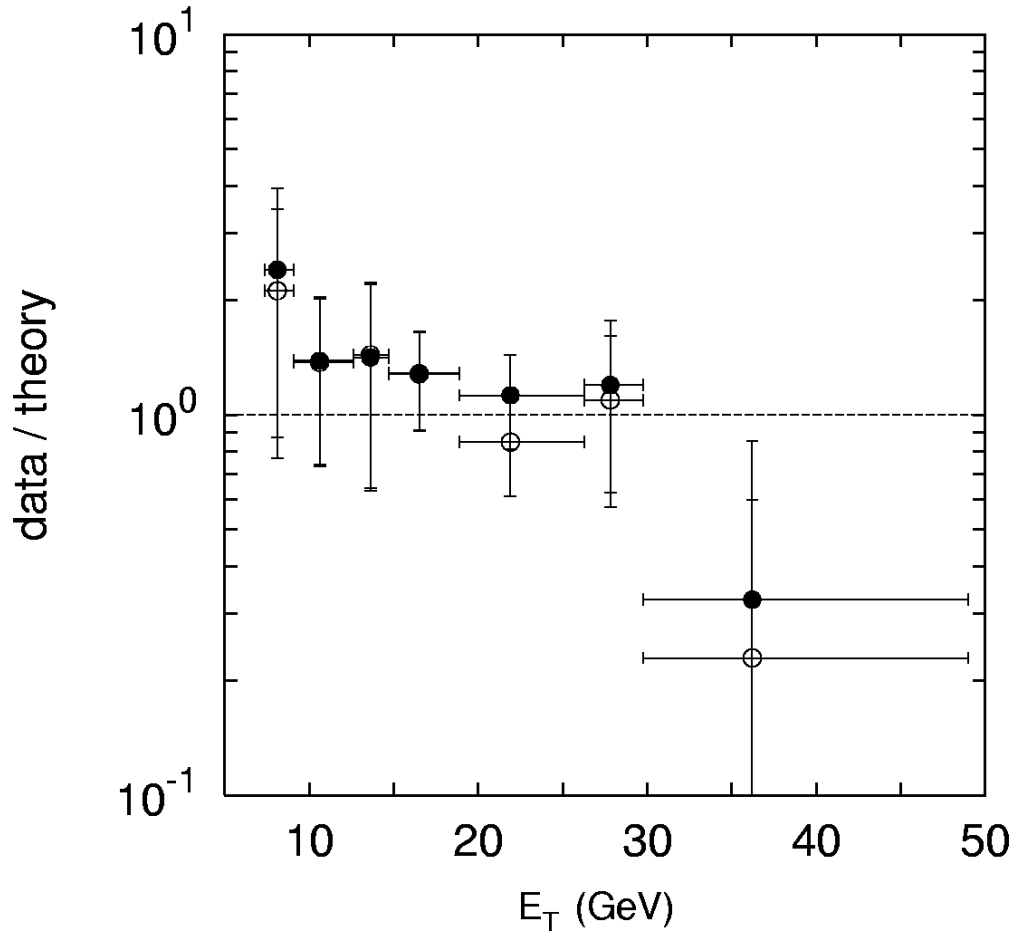


Figure 6: The data/theory ratio for inclusive prompt photon hadroproduction calculated at $1.6 < |\eta| < 2.5$ and $\sqrt{s} = 630$ GeV. Notations are the same as in Figure 5. The experimental data are from DØ [2].

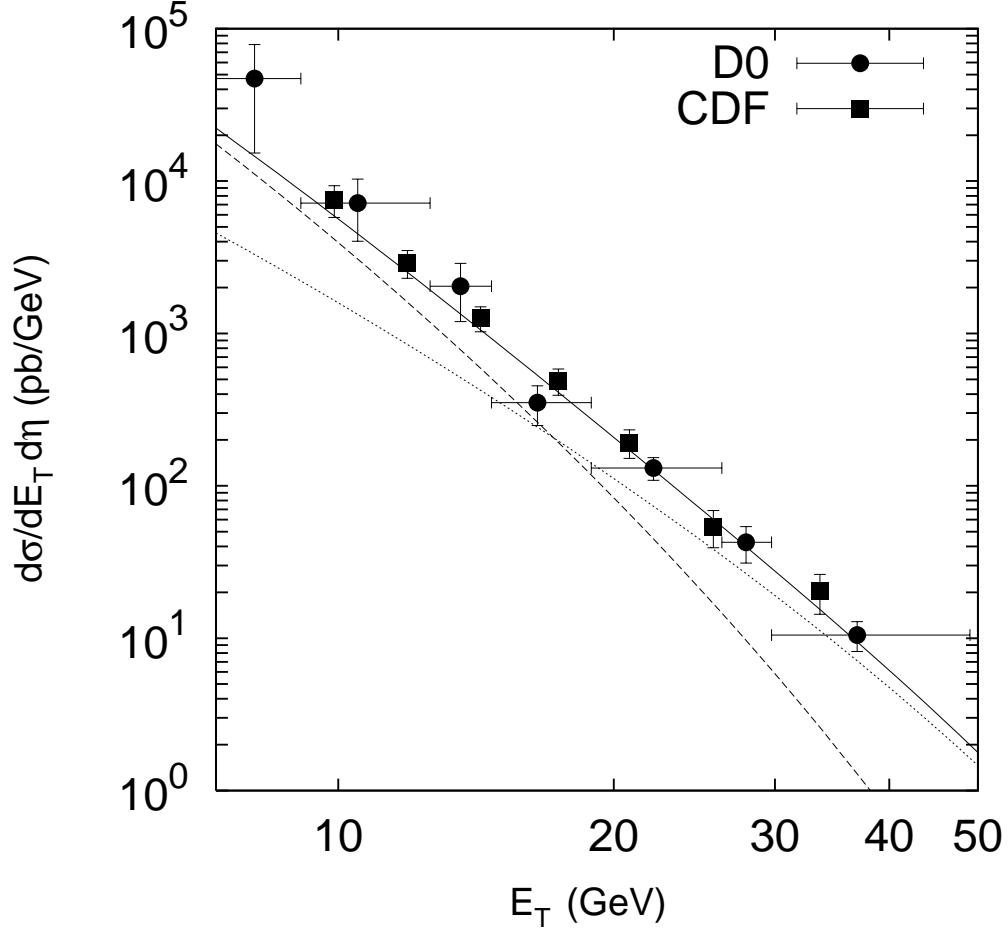


Figure 7: The double differential cross section $d\sigma/dE_T d\eta$ for inclusive prompt photon hadroproduction at $|\eta| < 0.9$ and $\sqrt{s} = 630$ GeV. The dashed and dotted lines represent the gluon and valence quark contributions to the prompt photon cross section, respectively. The solid line corresponds to the sum of these contributions. We have use here the CCFM gluon densities. The experimental data are from DØ [2] and CDF [3].

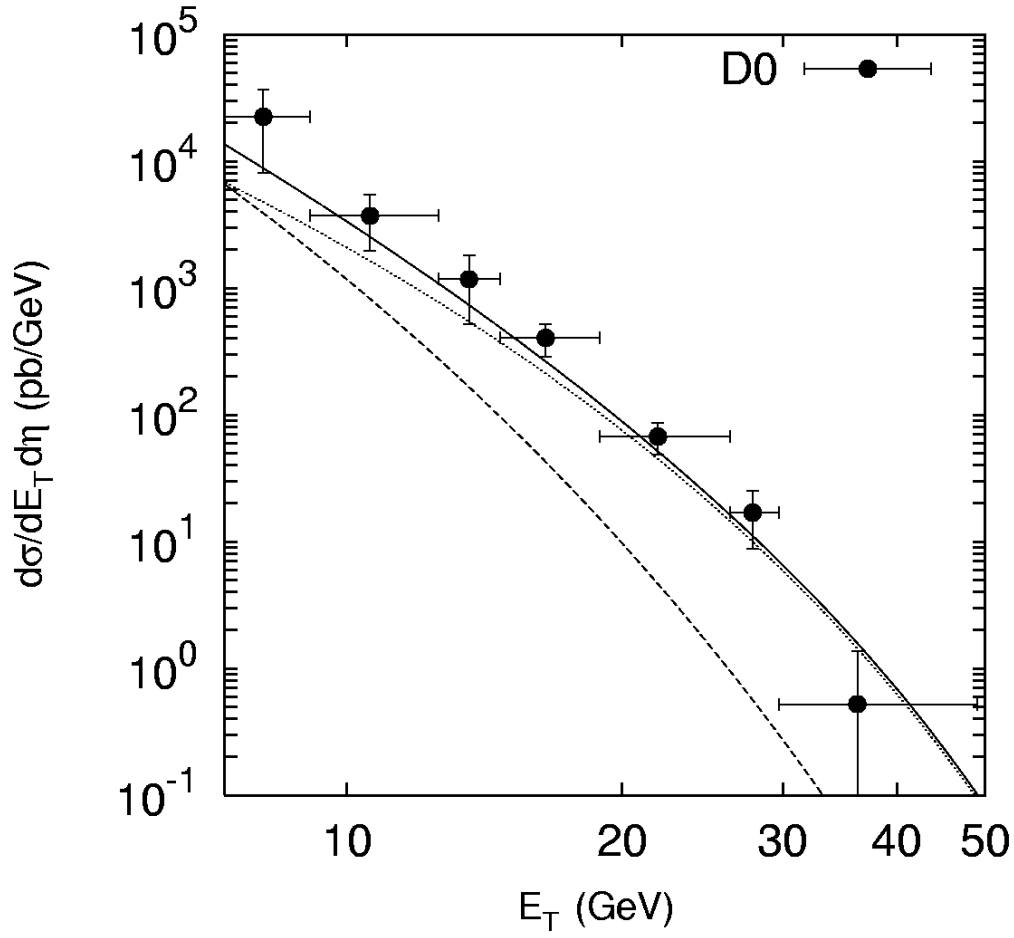


Figure 8: The double differential cross section $d\sigma/dE_T d\eta$ for inclusive prompt photon hadroproduction at $1.6 < |\eta| < 2.5$ and $\sqrt{s} = 630$ GeV. Notations of all curves are the same as in Figure 7. The experimental data are from DØ [2].

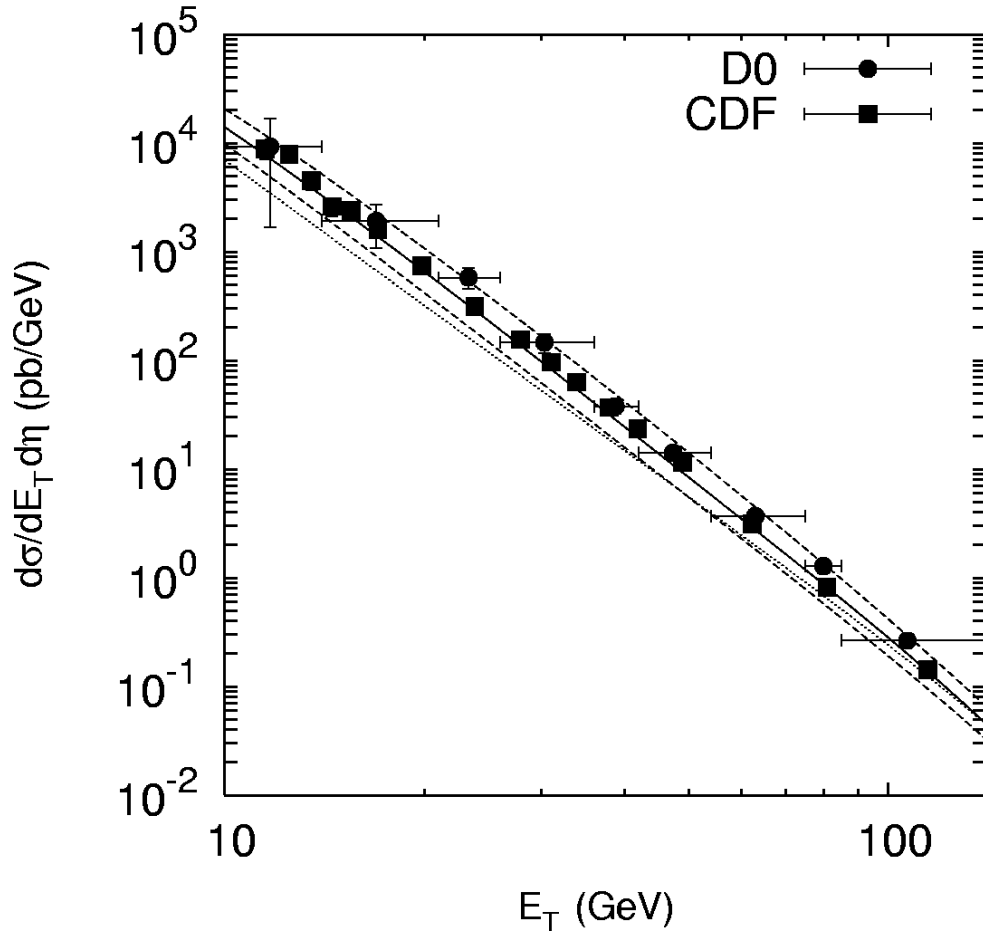


Figure 9: The double differential cross section $d\sigma/dE_T d\eta$ for inclusive prompt photon hadroproduction at $|\eta| < 0.9$ and $\sqrt{s} = 1800$ GeV. Notations of all curves are the same as in Figure 3. The experimental data are from D0 [1] and CDF [3, 4].

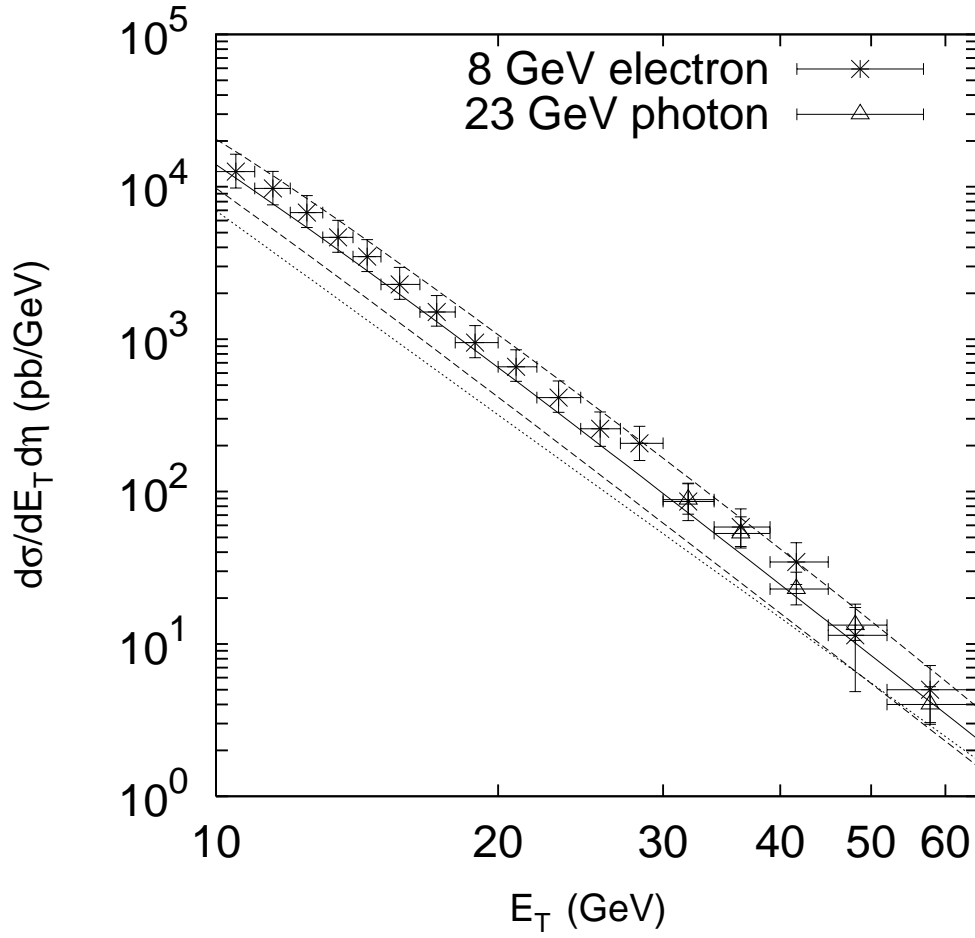


Figure 10: The double differential cross section $d\sigma/dE_T d\eta$ for inclusive prompt photon hadroproduction at $|\eta| < 0.9$ and $\sqrt{s} = 1800$ GeV. Notations of all curves are the same as in Figure 3. The experimental data are from CDF [5].

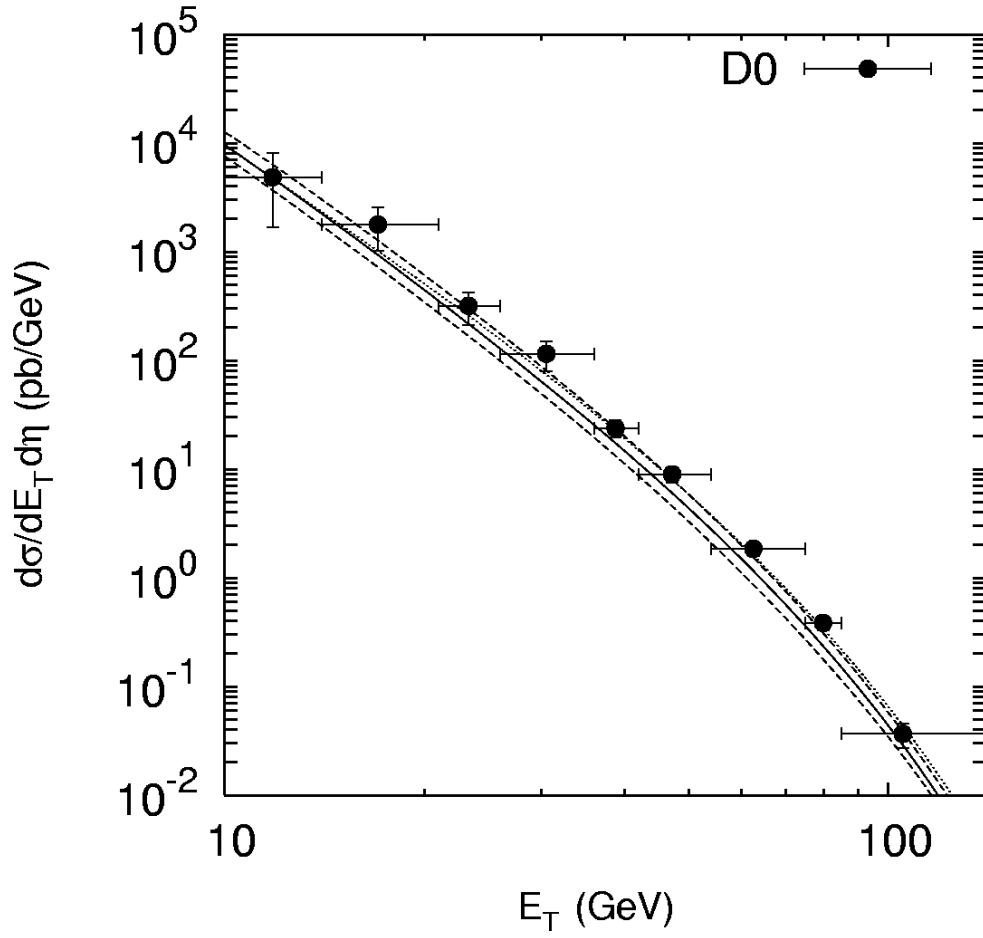


Figure 11: The double differential cross section $d\sigma/dE_T d\eta$ for inclusive prompt photon hadroproduction at $1.6 < |\eta| < 2.5$ and $\sqrt{s} = 1800$ GeV. Notations of all curves are the same as in Figure 3. The experimental data are from D0 [1].

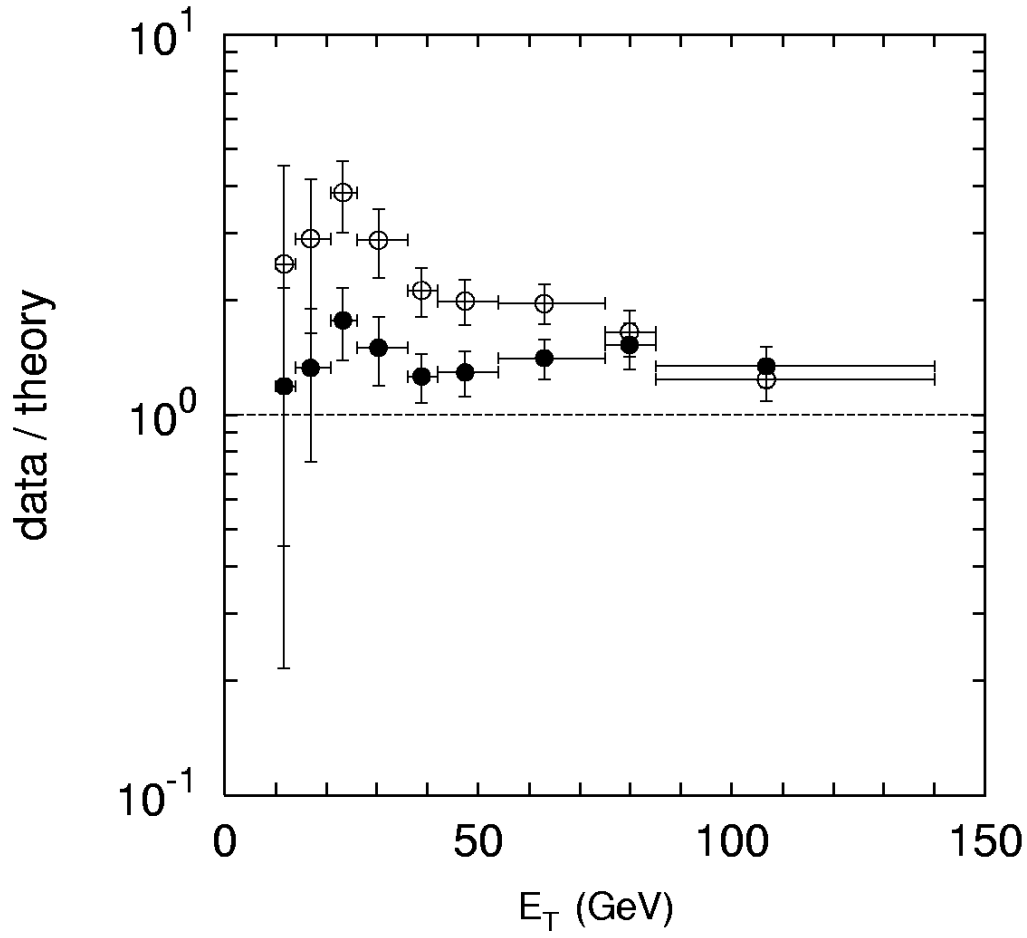


Figure 12: The data/theory ratio for inclusive prompt photon hadroproduction calculated at $|\eta| < 0.9$ and $\sqrt{s} = 1800$ GeV. Notations are the same as in Figure 5. The experimental data are from DØ [1].

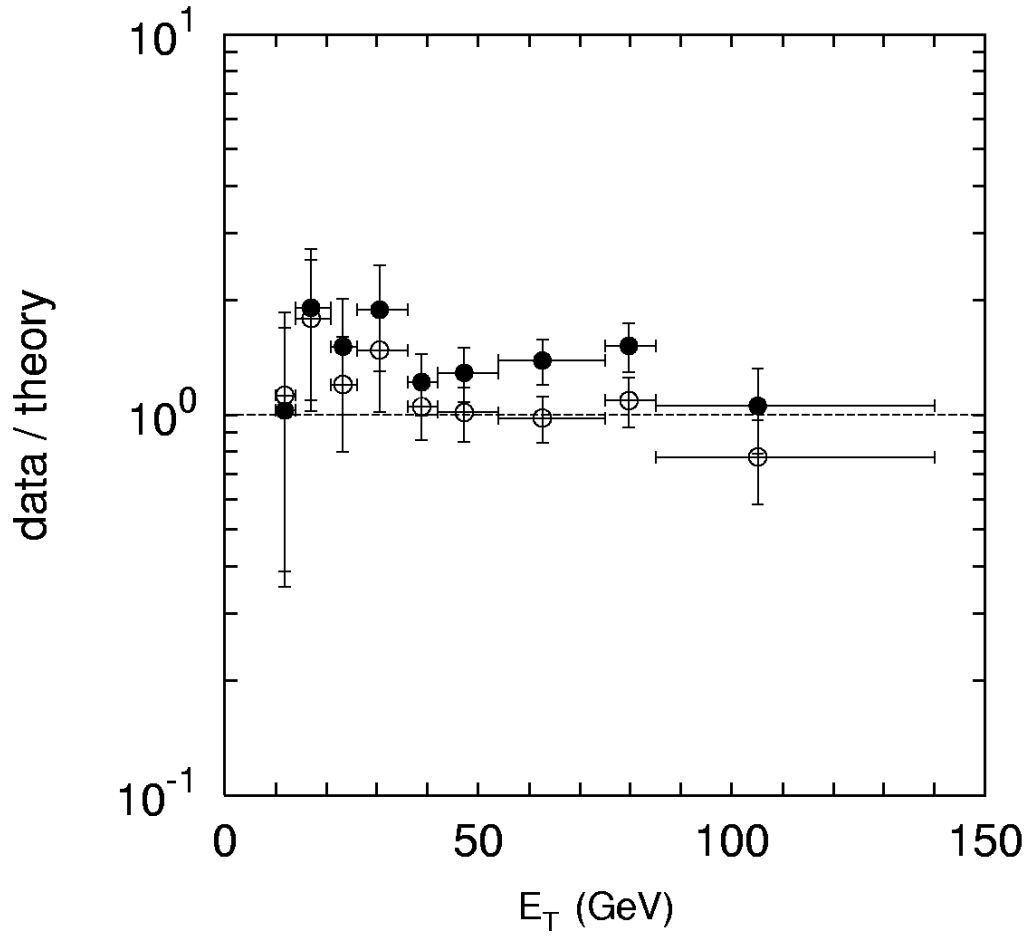


Figure 13: The data/theory ratio for inclusive prompt photon hadroproduction calculated at $1.6 < |\eta| < 2.5$ and $\sqrt{s} = 1800$ GeV. Notations are the same as in Figure 5. The experimental data are from DØ [1].

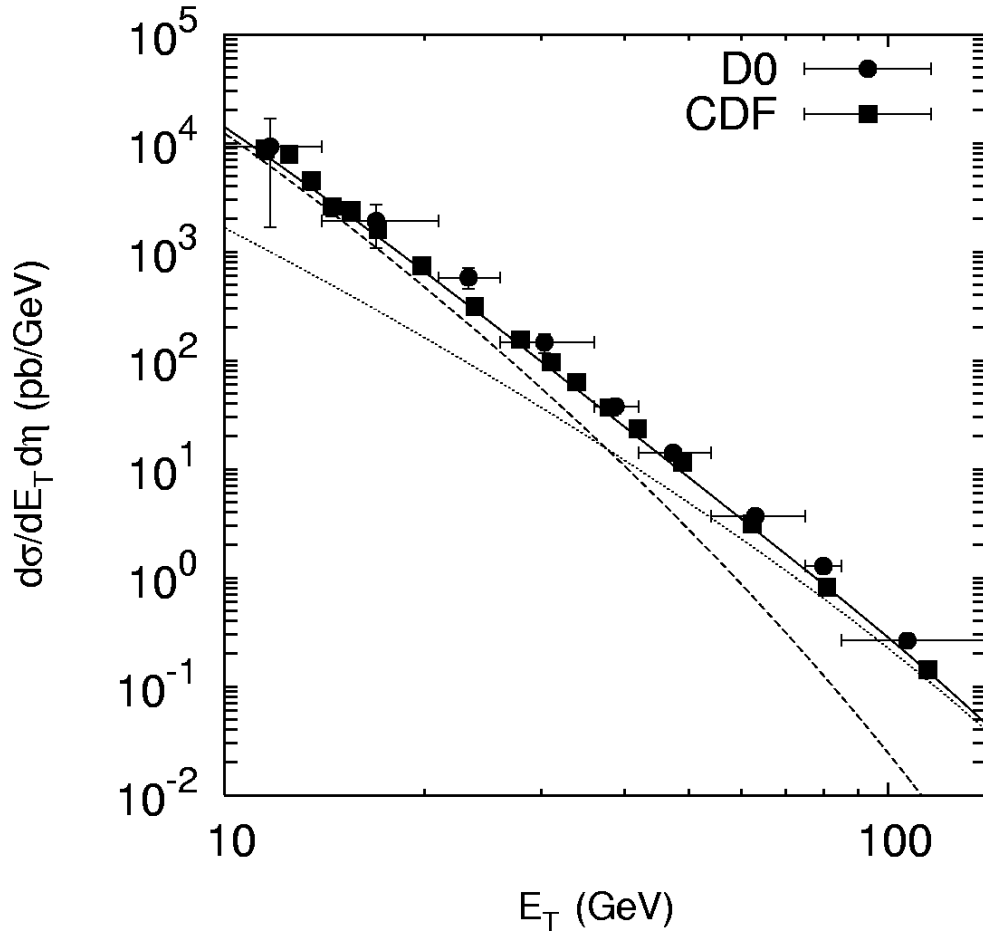


Figure 14: The double differential cross section $d\sigma/dE_T d\eta$ for inclusive prompt photon hadroproduction at $|\eta| < 0.9$ and $\sqrt{s} = 1800$ GeV. Notations of all curves are the same as in Figure 7. The experimental data are from D0 [1] and CDF [3, 4].

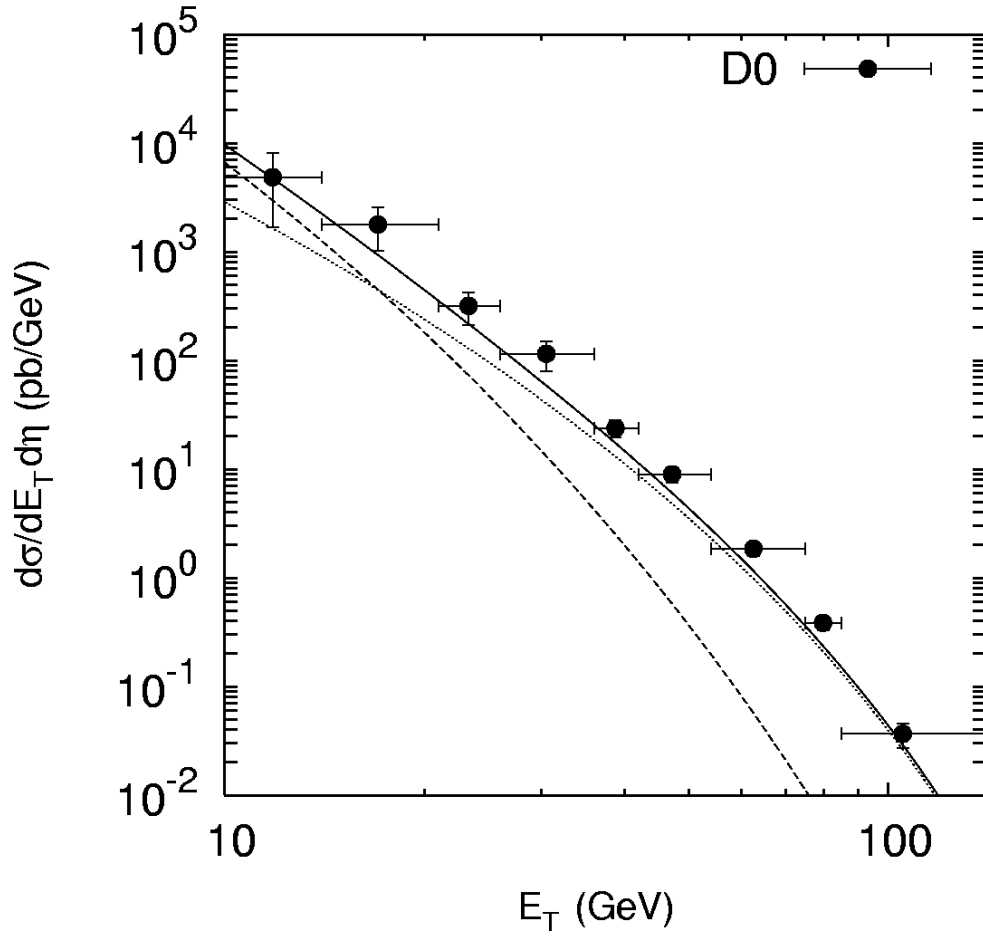


Figure 15: The double differential cross section $d\sigma/dE_T d\eta$ for inclusive prompt photon hadroproduction at $1.6 < |\eta| < 2.5$ and $\sqrt{s} = 1800$ GeV. Notations of all curves are the same as in Figure 7. The experimental data are from DØ [1].

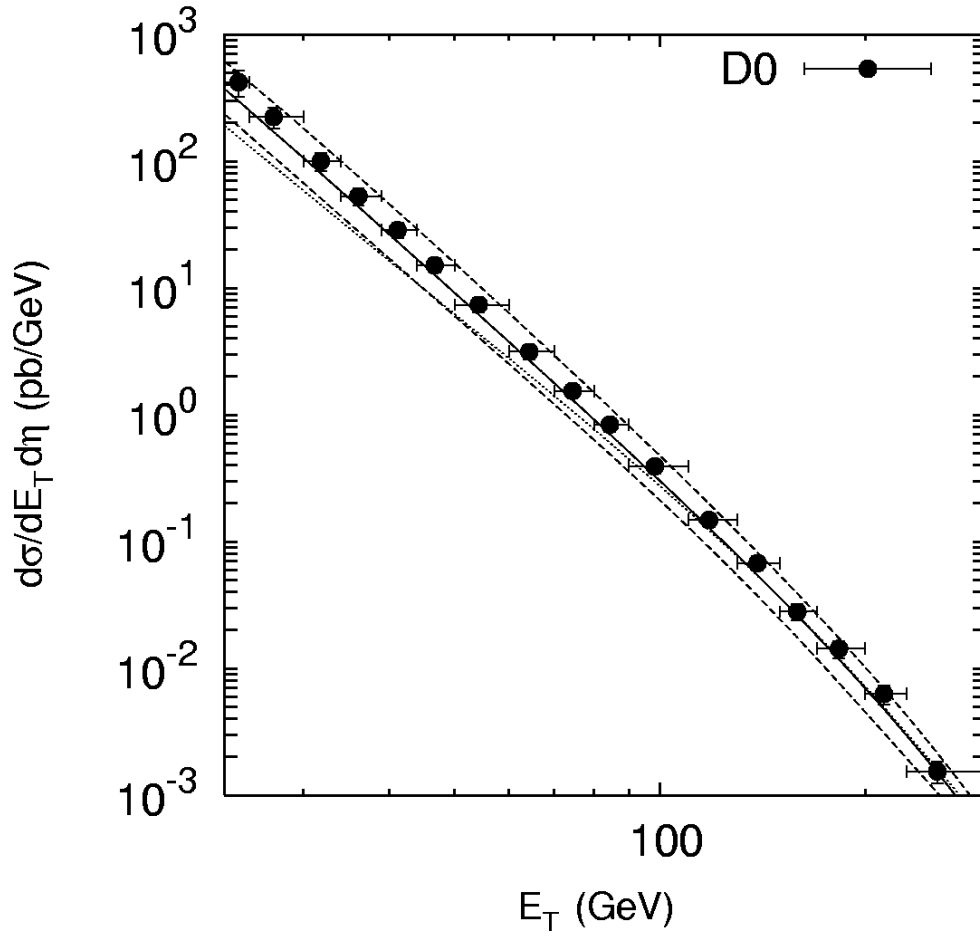


Figure 16: The double differential cross section $d\sigma/dE_T d\eta$ for inclusive prompt photon hadroproduction at $|\eta| < 0.9$ and $\sqrt{s} = 1960$ GeV. Notations of all curves are the same as in Figure 3. The experimental data are from D0 [6].

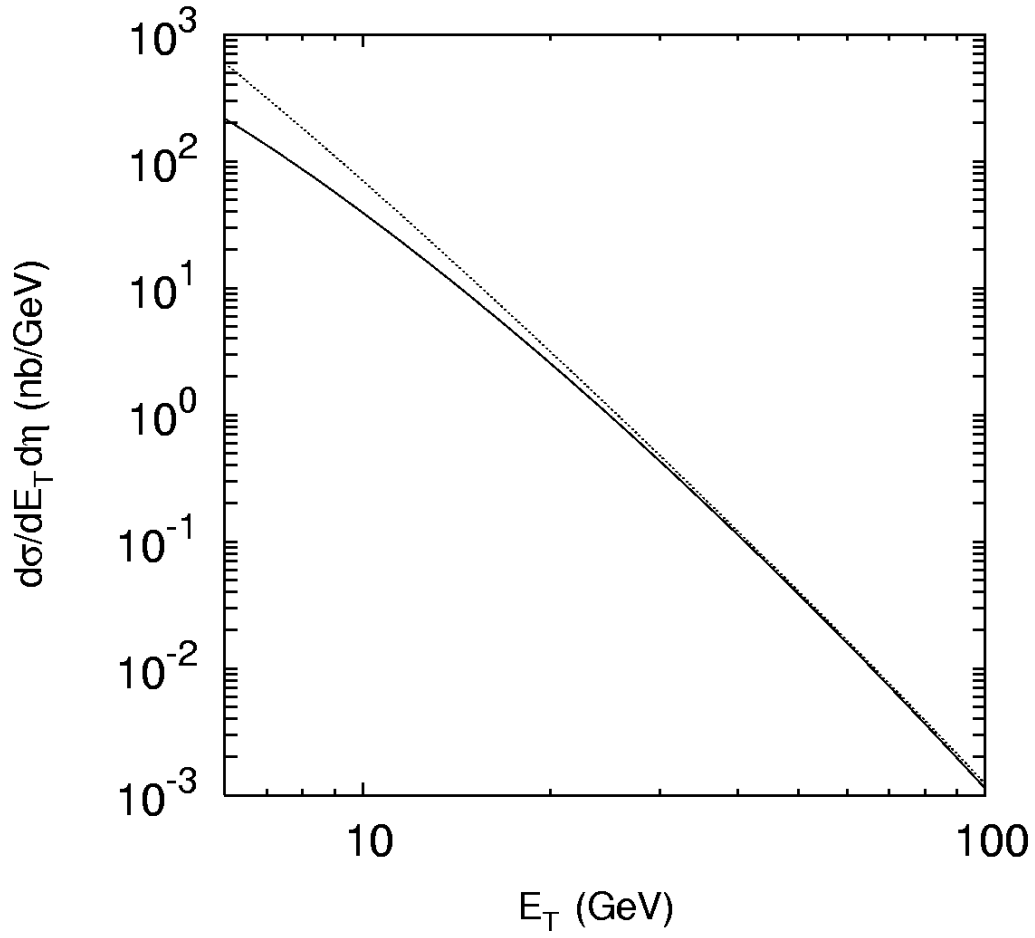


Figure 17: The transverse energy E_T distribution of inclusive prompt photon hadroproduction calculated at $|\eta| < 2.5$ and $\sqrt{s} = 14$ TeV. Notations of all curves are the same as in Figure 3.

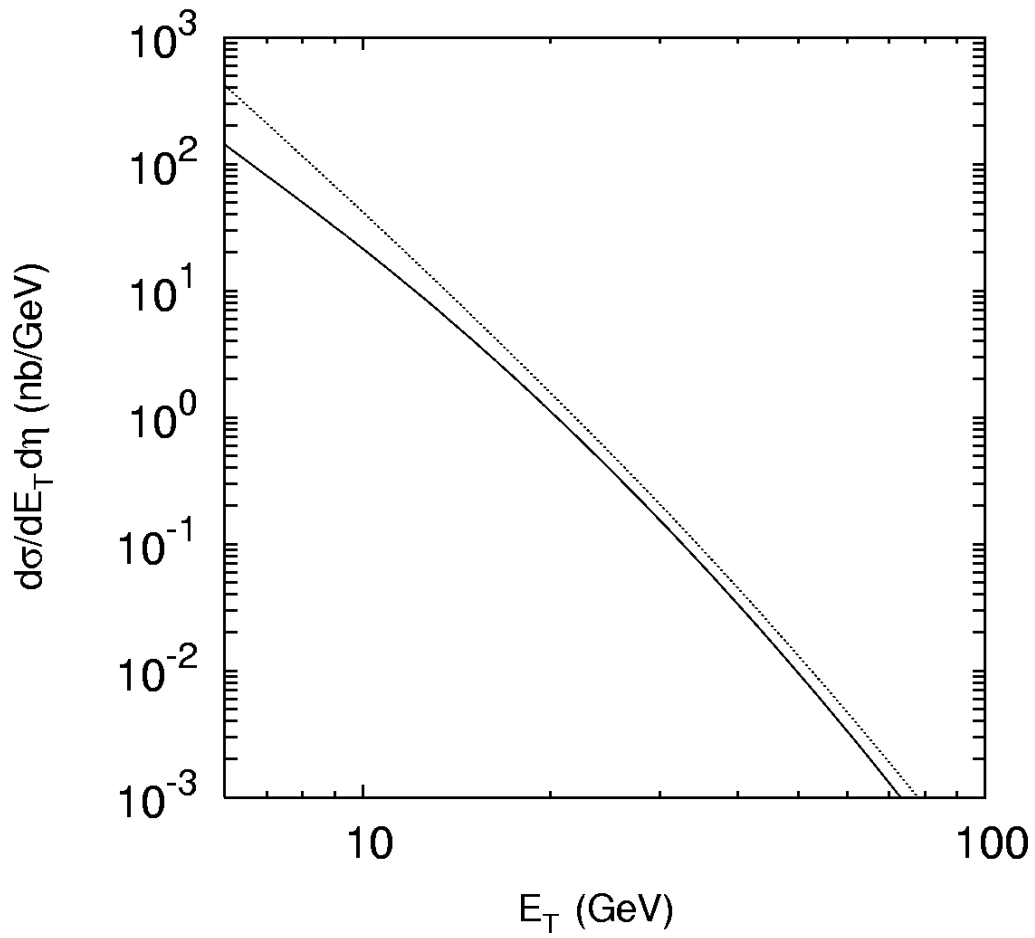


Figure 18: The transverse energy E_T distribution of inclusive prompt photon hadroproduction calculated at $2.5 < |\eta| < 4$ and $\sqrt{s} = 14$ TeV. Notations of all curves are the same as in Figure 3.